Complexes of HNgY with HX (Y, X = F, Cl, Br, I): Symmetry-Adapted Perturbation-Theory Study and Anharmonic Vibrational Analysis

Bartosz Dzięcioł[a,b], Irina Osadchuk[c], Janusz Cukras[a],* and Jan Lundell[c†]

[a] *Department of Chemistry, University of Warsaw, Poland*

[b] *Department of Physics, Graduate School of Science, The University of Tokyo, Faculty of Science, Japan*

[c] *Department of Chemistry, University of Jyväskylä, Finland*

(Dated: December 19, 2022)

Abstract

We performed the first comprehensive analysis of the intermolecular interaction energy and anharmonic vibrations of 41 structures of the HXeY$\cdots$HX (X, Y = F, Cl, Br, I) family of noble-gas-compound complexes for all possible combinations of Y and X. New structures are found and the interaction energy is studied by means of the symmetry-adapted perturbation theory up to the second-order corrections providing insight into the physical nature of the interaction in the complexes. The energy components are discussed in connection to anharmonic frequency analysis. The results show that the induction and dispersion corrections are the main driving forces of the interaction and their relative contributions correlate with the complexation effects seen in the vibrational stretching modes of Xe-H and H-X. Rather clear patterns of interaction are found for different structures. Our findings corroborate previous findings with better methods and provide new data. The results suggest that the entire group of the studied complexes can be labelled as "naturally blue-shifting" except for the complexes with HI.

I. INTRODUCTION

Although noble gases were long considered inert, we now know that they may form compounds which are interesting because of their octet-rule breaking origin. Compared to compounds formed by other elements, these compounds are not many, but the quest to find new ones continues since the seminal Neil Bartlett's discovery of the first xenon compound [1, 2]. Since then, many successful syntheses, as well as theoretical and computational developments have followed [3–6]. Among them, syntheses conducted in low-temperature matrices using a method developed in Helsinki [7–10].

The molecules synthesised in low-temperature matrices in Helsinki have the general formula HNgY where Ng denotes a noble-gas atom and Y is an electronegative group, e.g. F^-, Cl^-, OH^-. They are obtained by co-deposition of noble gas with HX precursor molecules (X = Cl, Br, I, OH etc.). After the deposition, the material is irradiated with ultraviolet (UV) radiation, leading to photodissociation of the precursor. The subsequent migration of mobile species induced by annealing reorganises the matrix, and as a result, HNgY molecules

* janusz.cukras@uw.edu.pl

† jan.c.lundell@jyu.fi

are formed. This method allowed the synthesis of the first ever compound of argon, namely the HArF molecule [11, 12]. From quantum-mechanical simulations it is known that the atoms in the positive $(H–Ng)^+$ part are covalently bonded [4, 7, 9, 13–16], although it is a charge-shift bond [15], whereas the bonding between the $(H–Ng)^+$ moiety and the negative Y^- moiety is predominantly of ionic nature.

Because these molecules are metastable, i.e. their structures do not represent global minima on the potential energy surface, they are very sensitive to their surroundings. This was immediately noticed in experiments and calculations. Attempts to simulate the condensed phase of HNgY molecules have been shown to be rather unsuccessful [17–19] and their complexes are predicted to have rather short lifetimes in room temperature. Larger complexes appear unstable and follow a rapid reaction through a two-body (2B: HNgY $\rightarrow$ HY + Ng) or a three-body (3B: HNgY $\rightarrow$ H + Ng + Y) decomposition channel [5, 18]. However, their complexation with a limited number of other molecules turned out to have a great stabilising effect on the HNgY molecule itself. This is evidenced by the fact that in the complexes, HNgY molecules typically exhibit a blue shift in the vibrational modes of ν_{HNg} [20] which is attributed to the strengthening of the H–Xe bond.

The subject of noble-gas compounds and especially their complexes is relevant in many fields. Despite the fact that some larger complexes of HNgY are predicted to be not very stable under normal conditions, their existence is still hypothesized in low-temperature stellar environments [19], high-pressure environments relevant to the geological question of missing xenon [21–23] and in phase boundaries. The ArH^+ molecular ion has been discovered in the Crab Nebula [24]. The properties of such species are important in the research of the history of interstellar matter. Molecular clouds have a temperature range of about 10–20 K, so even less stable noble gas compounds and complexes may be relevant for this field, especially because in such environments the chemical composition is not controlled thermodynamically [25]. Moreover, the properties and chemistry of gaseous xenon are important in Earthly conditions. Beside the missing xenon problem, xenon is known for its anesthetic properties [26, 27]. Despite many attempts to explain them, these properties are still mysterious and lack support from computational studies [28, 29]. If xenon penetrates cells to exert its anesthetic action, one may suppose that it can form short-lived compounds or complexes or even noble-gas-compound complexes in the phase-boundary-rich biochemical environment, interacting with cellular structures and influencing the biochemical equilibria of the living

cell [29].

Consequently, since the study of xenon properties has the greatest implications, its compounds have received the most attention. Xenon has the highest polarizability among noble gases and, due to this fact, it was predicted early to be able to form compounds [30] and it indeed forms the largest number of compounds and complexes compared to other noble-gas elements, including the HXeY family of compounds. Among them, the HXeOH molecule has been studied extensively [10, 14, 17–19, 31]. The different properties of other complexes have also received considerable attention, both experimentally and computationally. For instance, the body of research encompasess HXeCl/Br/I$\cdots$$H_2O$ [32, 33], HXeCl/Br$\cdots$HCl/Br [20, 34], HXeI$\cdots$HBr/I [35], HXeI$\cdots$HCl and HXeI$\cdots$HCCH [36], $(HXeF)_2$ and $(HXeF)_3$ [37], HXeF$\cdots$HF [13, 34, 38], HXeBr/Cl$\cdots$HCl/Br and HXeCCH$\cdots$$CO_2$ [14], HXeBr$\cdots$$CO_2$ [39], HXeSH$\cdots$$H_2O$/$H_2S$ [40], HXeOH$\cdots$$H_2S$. Recently, Zhang et al. [15] have investigated a large set of systems, i.e. HXeY$\cdots$HX (Y=Cl/Br/I and X=OH/Cl/Br/I/CCH/CN) and have established the charge-shift nature of the H-Xe bonding in the noble-gas molecule.

Although there exists a rich literature on chosen aspects of the chosen HXeY$\cdots$HX complexes and their groups, a comprehensive analysis of the physics of the interaction encompassing all combinations of Y and X moieties is missing. In this study, we aim to fill this gap by providing a description of the nature of the interaction in the complexes of the family of HXeY compounds (Y=F, Cl, Br, I) with the series of hydrogen halide molecules HX (X=F, Cl, Br, I) using the symmetry-adapted perturbation theory [41] as well as combining this description with anharmonic frequency analysis, with particular focus on the complexation effects on the Xe-H and H-X stretching modes, which are of special importance for the interpretation of the experimental spectra. In our analysis, we include the high-energy structures of complexes, i.e. the structures of local minima, since the noble-gas low-temperature matrices, as opposed to e.g. nitrogen matrices, tend to preserve the different gas-phase structures of complexes by trapping them among noble-gas atoms and interaction strength tends to be enhanced in the matrix [42].

The subject of noble-gas compounds and especially their complexes is relevant in many fields. Despite the fact that some larger complexes of HNgY are predicted to be not very stable under normal conditions, their existence is still hypothesized in low-temperature stellar environments [19], high-pressure environments relevant to the geological question of missing xenon [21–23] and in phase boundaries. The ArH^+ molecular ion has been discovered in the

Crab Nebula [24]. The properties of such species are important in the research of the history of interstellar matter. Molecular clouds have a temperature range of about 10–20 K, so even less stable noble gas compounds and complexes may be relevant for this field, especially because in such environments the chemical composition is not controlled thermodynamically [25]. Moreover, the properties and chemistry of gaseous xenon are important in Earthly conditions. Beside the missing xenon problem, xenon is known for its anesthetic properties [26, 27]. Despite many attempts to explain them, these properties are still mysterious and lack support from computational studies [28, 29]. If xenon penetrates cells to exert its anesthetic action, one may suppose that it can form short-lived compounds or complexes or even noble-gas-compound complexes in the phase-boundary-rich biochemical environment, interacting with cellular structures and influencing the biochemical equilibria of the living cell [29].

Consequently, since the study of xenon properties has the greatest implications, its compounds have received the most attention. Xenon has the highest polarizability among noble gases and, due to this fact, it was predicted early to be able to form compounds [30] and it indeed forms the largest number of compounds and complexes compared to other noble-gas elements, including the HXeY family of compounds. Among them, the HXeOH molecule has been studied extensively [10, 14, 17–19, 31]. The different properties of other complexes have also received considerable attention, both experimentally and computationally. For instance, the body of research encompasess HXeCl/Br/I$\cdots$$H_2O$ [32, 33], HXeCl/Br$\cdots$HCl/Br [20, 34], HXeI$\cdots$HBr/I [35], HXeI$\cdots$HCl and HXeI$\cdots$HCCH [36], $(HXeF)_2$ and $(HXeF)_3$ [37], HXeF$\cdots$HF [13, 34, 38], HXeBr/Cl$\cdots$HCl/Br and HXeCCH$\cdots$$CO_2$ [14], HXeBr$\cdots$$CO_2$ [39], HXeSH$\cdots$$H_2O$/$H_2S$ [40], HXeOH$\cdots$$H_2S$. Recently, Zhang et al. [15] have investigated a large set of systems, i.e. HXeY$\cdots$HX (Y=Cl/Br/I and X=OH/Cl/Br/I/CCH/CN) and have established the charge-shift nature of the H-Xe bonding in the noble-gas molecule.

Although there exists a rich literature on chosen aspects of the chosen HXeY$\cdots$HX complexes and their groups, a comprehensive analysis of the physics of the interaction encompassing all combinations of Y and X moieties is missing. In this study, we aim to fill this gap by providing a description of the nature of the interaction in the complexes of the family of HXeY compounds (Y=F, Cl, Br, I) with the series of hydrogen halide molecules HX (X=F, Cl, Br, I) using the symmetry-adapted perturbation theory [41] as well as combining this description with anharmonic frequency analysis, with particular focus on the complexation

effects on the Xe-H and H-X stretching modes, which are of special importance for the interpretation of the experimental spectra. In our analysis, we include the high-energy structures of complexes, i.e. the structures of local minima, since the noble-gas low-temperature matrices, as opposed to e.g. nitrogen matrices, tend to preserve the different gas-phase structures of complexes by trapping them among noble-gas atoms and interaction strength tends to be enhanced in the matrix [42].

II. COMPUTATIONAL METHODS

Geometry optimisation was performed using many starting molecular orientations of the HX and HXeY molecules with the aim of finding as many local minima as possible. Vibrational analysis was performed on the converged structures to exclude transition states. Anharmonic frequencies were also obtained. These procedures were performed using density functional theory with the B3LYP functional. The above calculations were performed in Gaussian'09 [43].

Further calculations were intended to determine the supermolecular intermolecular interaction energy and the physical nature of interactions by means of symmetry-adapted perturbation theory (SAPT) [41] as implemented in the MOLPRO software suite [44].

Preceding the computations of the intermolecular interaction energies, additional geometry optimisation was applied to previously found structures, this time using the Second-Order Møller-Plesset perturbation theory (MP2) in the Gaussian programme suite. Not all structures previously found were successfully optimised, including most of the structures with linear geometry (later denoted as structures of type 2a, see Section III A). For some of the uncertain structures, additional calculations were performed using "very tight" convergence criteria. The nature of all minima was established by vibrational analysis yet again, and anharmonic frequencies were calculated as well. Only anharmonic vibrational frequencies are discussed herein and presented in the tables.

For hydrogen, fluorine, and chlorine, the Dunning-type singly augmented aug-cc-pVTZ basis set was employed [45–48], meanwhile, for the heavier elements, i.e. bromine, iodine, and xenon, the used basis set was aug-cc-pVTZ-PP [49, 50] which takes into account the scalar relativistic effect employing the effective core potentials (ECP). The basis sets were obtained from the Basis Set Exchange (BSE) library [51].

The supramolecular interaction energy was obtained with different levels of theory by standard approach, i.e. subtracting the total energies of the constituent species from the total energy of the complex:

$$E_{\mathrm{int}}^{\mathrm{method}} = E_{\mathrm{A+B}}^{\mathrm{method}} - E_{\mathrm{A}}^{\mathrm{method}} - E_{\mathrm{B}}^{\mathrm{method}} \tag{1}$$

taking into account the basis-set superposition error by using full basis set of the complex for the energy calculations of the monomers [52]. The employed methods include the Hartree-Fock method (HF), the second and fourth order Møller-Plesset Perturbation Theory (MP2 and MP4), the Coupled-Cluster Singles and Doubles (CCSD) and Coupled-Cluster Singles Doubles with Perturbative Triples (CCSD(T)). Zero-Point Energy (ZPE) corrections were not employed, and neither have been the corrections for geometry deformation upon complexation.

At the level of theory used, the SAPT interaction energy has the following components:

$$E_{\mathrm{int}}^{\mathrm{SAPT0}} = E_{\mathrm{elst}}^{(10)} + E_{\mathrm{exch}}^{(10)} + E_{\mathrm{ind,r}}^{(20)} + E_{\mathrm{exch-ind,r}}^{(20)} + E_{\mathrm{disp}}^{(20)} + E_{\mathrm{exch-disp}}^{(20)} + \delta E_{\mathrm{int,resp}}^{\mathrm{HF}}, \tag{2}$$

where $E_{\mathrm{elst}}^{(10)}$ is electrostatic energy, $E_{\mathrm{exch}}^{(10)}$ is exchange energy, $E_{\mathrm{ind,r}}^{(20)}$ is induction energy, $E_{\mathrm{exch-ind,r}}^{(20)}$ is coupling between exchange and induction energy, $E_{\mathrm{disp}}^{(20)}$ is dispersion energy, $E_{\mathrm{exch-disp}}^{(20)}$ is coupling between exchange and dispersion energy and $\delta E_{\mathrm{int,resp}}^{\mathrm{HF}}$ is assumed to include mainly the third-order induction term.

The above terms were arranged as follows for our analysis:

$$E_{\mathrm{elst}} = E_{\mathrm{elst}}^{(10)}$$

$$E_{\mathrm{exch}} = E_{\mathrm{exch}}^{(10)}$$

$$E_{\mathrm{ind}} = E_{\mathrm{ind,r}}^{(20)} + E_{\mathrm{exch-ind,r}}^{(20)} + \delta E_{\mathrm{int,resp}}^{\mathrm{HF}}$$

$$E_{\mathrm{disp}} = E_{\mathrm{disp}}^{(20)} + E_{\mathrm{exch-disp}}^{(20)}$$

$$E_{\mathrm{tot}}^{\mathrm{int}} = E_{\mathrm{tot}}^{1+2} = E_{\mathrm{elst}} + E_{\mathrm{exch}} + E_{\mathrm{ind}} + E_{\mathrm{disp}}$$

and plotted in the form of bar graphs.

All data analysis and visualization was performed using iPython and Jupyter Notebooks [53, 54], Matplotlib [55], and Pandas [56, 57] packages.

III. RESULTS

A. Structures

Geometry optimization provided five different structure types for most of the compositions of the complexes and they are depicted in Fig.1. We may distinguish:

1. type 1 structure where the hydrogen atom of HX is directed away from the noble-gas molecule and the halogen atoms are neighboring each other; there is no hydrogen bond;

2. type 2 structure which is a bent hydrogen-bonded structure where the hydrogen atom of the noble-gas molecule is involved in the hydrogen bonding; HNgY is the proton-donor;

3. type 2a structure which is the same as type 2 but it is linear; HNgY is again the proton-donor;

4. type 3 structure which is similar to type 1 but the orientation of the HX molecule is reversed and its hydrogen atom points toward the halogen atom of the noble-gas molecule, forming hydrogen bond; HX is the proton-donor;

5. type 3a structure which is similar to type 3 but the angle formed between both interacting molecules is larger; HX is the proton-donor.

Some of the investigated structures were previously reported and studied experimentally and computationally [13, 14, 34, 36, 38, 40]. Zhang et al. [15] have recently studied the H-Xe bonding in all these structures except 2a and 3a for Y and X = Cl, Br, I. Our structural results are in excellent agreement with these previous reports.

Since a given composition of the studied complexes can assume different structures, we indicate the structure of the composition by its type following the formula, i.e. $HXeY\cdots HX/n$,

where n is the structure type. For instance, HXeCl$\cdots$HBr/2 for the complex of HXeCl molecule with HBr molecule with both molecules arranged in type 2 geometry.

B. The total intermolecular interaction energy values

The supermolecular interaction energy values and the total SAPT interaction energy values are given in Table I. Let us focus on the MP2 supermolecular energies. It can be seen that structures of type 3 and 3a have the lowest values, ranging from ca. -20 to ca. -60 kJ mol^{-1} and can generally be considered the most stable. Next in terms of stability are those of structures of type 1 which involve heavier halogen atoms in the HX unit, from ca. -10 to ca. -14 kJ mol^{-1}. Structures of type 1 with light halogen atoms in HX and structures of type 2 have the highest interaction energy value, ca. -4 to ca. -6 kJ mol^{-1} and structures of type 2 are bound the weakest.

In Tab. I, one can clearly see that the total interaction energies for all structures 2 are very close to each other and the same can observed for group 3. Independent of the ingredients of the complex and excluding complexes containing HF, the energies range from ca. -20 to ca. -30 kJ mol^{-1} for structures 3 and from ca. -4 to ca. -6 kJ mol^{-1} for structures 2. Meanwhile, the energies for structures 1 are very different and clearly increase when going from HF to HI (with the exception of HXeF). The cause for this different trend seems to be the difference in the origin of the interaction.

As can be seen in Fig. 1, all the structure types except 1 are formed with hydrogen bonding. The hydrogen bond in structures 3 and 3a is strong because it is formed between strongly negative Y^- moiety of the noble-gas molecule and the hydrogen atom of the HX molecule, that is, the HX molecule is the proton donor. The magnitude of this interaction is comparable to the interaction in the water dimer [58, 59]. The hydrogen bonds in structures 2 are weaker because the noble-gas molecule is the proton donor and it has been shown [14] that complexation has a shortening effect on $r_{\mathrm{H-Ng}}$ making it a worse proton donor. Because of the unfavorable orientation, the interaction is, thus, smaller. However, the interaction itself is of comparable magnitude within the entire group 2.

Conversely, the interaction origin for structures of type 1 are different. As we can see on Fig. 1(a), the interaction arises from the vicinity of the halogen atoms of both interacting molecules, thus the interaction energy is different for each interacting case. It systematically

increases with the atomic number of the halogen atom in the HX molecule but for a given HX molecule it remains remarkably constant when changing the halogen atom in the HXeY molecule. This means that the magnitude of the interaction energy in structures of type 1 is primarily governed by the type of HX molecule.

Let us now compare the energy trend within each group separately. In the case of group 3, we can see that the total energy slightly increases (i.e. is less stabilizing) when going from HF to HI for a given noble-gas molecule. This correlates well with the decreasing dipole moment in the sequence of HF-HCl-HBr-HI. This trend is, however, reversed in structures of type 1 and 2. This might be caused by the relative orientation of the dipole moments of both molecules and is discussed later in Section III C in terms of SAPT contributions to the interaction energy.

In summary, the hydrogen-bonded complexes tend to have intermolecular interactions of comparable size for a given geometry independent of the composition, whereas the magnitude of the interaction for the complexes interacting via halogen atoms varies depending on the halogen hydride.

It must be noted that complexes containing fluorine atom are often exception to these considerations. The HXeF$\cdots$HF complex was previous computationally reported by Jankowska and Sadlej [38] and by Mohajeri and Bitaab [13] in the forms of structures 3 and 2a. Jankowska has obtained -63.99 kJ mol^{-1} for structure of type 3 and -8.18 kJ mol^{-1} for structure of type 2a with the MP2 method. Mohajeri reports -56.94 kJ mol^{-1} for structure 3 with DFT/BMK approach. Our results agree with their data giving the value of -62.99 kJ mol^{-1} at MP2 level of theory. The results discussed are also in agreement with previous studies of the complexes of HXeBr and HXeCl molecules [14, 20].

C. The SAPT analysis of the intermolecular interaction energy

Let us now move on to discussion of the different terms as obtained by the SAPT method. Except for structures containing fluorine, all the studied complexes have a repulsive sum of first-order SAPT energies, i.e., the electrostatic and exchange interactions are not sufficient to explain the found minima. This means that they are stabilized by higher-order interaction terms, namely, the induction and dispersion.

The results are presented in a group-wise manner, following the structure types indicated

in section III A. The numerical results of the total SAPT energy are presented in Table I. Furthermore, we prepared three types of graphs to ease different types of comparisons. In Figures 2 to 5, we present values for different energy terms for the complexes grouped by the HX molecule. On Figures 6 to 8 we present the same results arranged by the HXeY molecule (2a and 3a results were not rearranged due to their limited number). In the Appendix, in Figures 9 to 15, we present the relative values of different components of the interaction energy, meaning that each individual term was divided by E_{tot}^{1+2} prior to plotting, the total SAPT interaction energy being represented by 1. This gives insight into the nature of the interaction, abstracting from the magnitude of the interaction as a whole which might be understood as a qualitative "fingerprint" of the interaction.

The SAPT contributions to the total interaction energy of structures of group 1 are presented on Figs. 2 and 6. In this type of geometry, the HX molecule faces the halogen atom of HXeY and the Xe–Y$\cdots$X angle is acute (see Fig. 1a). The main sources of stabilization are the electrostatic and dispersive terms, while induction plays a minor role. Dispersion is clearly the dominant 2nd order contribution to the interaction energy. For a given HX molecule, the individual contributions remain remarkably constant. For a given HXeY molecule in this structure type, the electrostatic, exchange and dispersion terms increase significantly when changing the mass of HX which produces the increasing total interaction energy. This is in line with our supermolecular results (see Section III B).

Relative contributions to the total interaction energy provide a qualititave picture of the interaction energy composition, i.e. a fingerprint of the interaction type. The relative contributions are depicted in Fig.9 and 15. One can see that the fingerprint remains generally the same for all these structures, independent of the composition.

The low induction contribution might come as a surprise because the noble-gas molecules have large dipole moments, however, one may note that the dipole moments of both interacting molecules point towards similar directions, i.e. no large dipole moment induction should be expected. Thus, there are no co-operative forces to induce additional partial charges.

This is in stark contrast to what we observe for energy partitioning in the case of structures of type 3. The structures marked with number 3 generally have the lowest total interaction energy which makes them potentially the most stable. Their SAPT energies are presented on plots 4 and 8. In these geometries, the hydrogen atom from HX faces the halogen atom from HXeY and the Xe–Y$\cdots$H angle is acute (Fig.1d). These structures have a hydrogen bond

HXeY$\cdots$HX interaction, however, since they are bent, a larger interaction between entire constituent molecules is expected as well. This is evidenced by the bar graphs in Fig. 4. One can see that the first order energies provide little stabilizing effect or they are destabilizing while the second-order induction and dispersion provide crucial attractive contributions to the total interaction. This shows that the complexes of type 3 are induction-dispersion-stabilised while the induction plays the leading role in most of the structures. The role of dispersion increases with the atomic number of the halogen atom. In general terms, however, the magnitude of the induction and dispersion interactions is comparable for all structures of type 3 (especially for a given HXeY molecule, and with the exception of those containing F) and one can conclude that the observed weakening of the total interaction when going from HF to HI is caused by the increasing electrostatic and exchange terms. The same trend can be observed for a fixed HX.

The relative contributions of the individual terms to the total interaction (see. Fig.11) are also quite similar for all the structures of type 3 but we can notice a slight variability in dispersion-to-induction ratio, as noted above. The ratio changes from ca. 0.5 to ca. 1.33. Summarizing these trends, one can tell that the share of E_{disp} when compared to E_{ind} is the highest for the structure HXeI$\cdots$HI and the lowest for HXeF$\cdots$HF. Additionally, for structures of type 3, both the induction and dispersion interactions are the largest compared to the other groups of the studied complexes.

In the same way as the small induction terms can be rationalized by the orientation of the interacting molecules for the structures of type 1, the large induction interaction for structures 3 may be explained by the dipole moments being oriented in an advantageous manner relative to each other, i.e. they are close to antiparalell orientation.

Let us now move on to the structures marked with number 2. Their SAPT energy contributions are presented on plots 3 and 7. Out of all considered types of structures, they have the highest total energy in general and so are potentially the least stable complexes. The halogen atom of HX faces the hydrogen atom of HXeY while the angle H-X$\cdots$H is close to 90 degrees (see Fig.1b). The structures are stabilised by electrostatic, induction and dispersion energies, with the shares of all three being important. However, since the electrostatic term is again quenched by the exchange interaction, we conclude that the stabilisation of these complexes arises mostly from the second-order corrections, i.e. dispersion and induction, but unlike in the case of structures of type 3, structures of type 2 are clearly dominated by

the dispersion contribution. Both induction and dispersion fall in the order from HF to HI for the structures with a given HXeY. Similarly, both energy contributions fall in order from HXeF to HXeI for the structures with a given HX, but this fall is generally smoother and there are exceptions. With the exception for structures with HXeF, the relative contribution of induction (see Fig.14) and dispersion rises slightly in the order from HF to HI. On the relative graphs one can observe yet again that the overall fingerprint of the interaction remains similar for all the structures of type 2.

These energetic characteristics of structure of type 1, 2 and 3 are in agreement with previous report for HXeY$\cdots$HX for X, Y = Cl and Br (see Tab. 4 in Ref. [14]), however, direct comparison is difficult because of different methodology employed, namely the Morokuma analysis. The present results show the trends in energy decomposition apply to different compositions of the complexes and depend mostly on the geometry.

The structures marked as 2a are similar to the structures marked as 2, that is, the HX halogen atom faces the hydrogen atom of HXeY but the structure is linear, that is, the angle H–X$\cdots$H is close to 180 degrees (see Fig. 5). Only two structures of this kind have converged, both containing HF. The relative share of electrostatic energy is much higher than the share of dispersion and induction energies. The structure with HXeCl has a lower total interaction energy as well as all the other components. The destabilisation coming from the exchange energy is greater for this structure as well. One can also notice that the share of the induction energy compared to the dispersion energy is much higher for the structure with HXeCl (see Fig.12).

Analogically, the structures marked 3a are similar to the structures marked 3, the only difference is that the Xe–Y$\cdots$H angle is obtuse. The same two structures containing HF have successfully converged. Again, the share of electrostatic energy is much higher than the share of dispersion and induction energies. This time the structure with HXeCl has higher total energy which makes it potentially less stable. The induction and electrostatic energies are clearly higher in the structure with HXeF, whereas the dispersion energy is lower. The destabilisation coming from the exchange energy is lower as well. The share of induction compared to dispersion is significantly lower for the structure containing the HXeCl molecule.

D. Vibrational spectroscopy

Now, we proceed to the discussion of the anharmonic vibrational modes. We will focus on these features of the vibrational spectrum that are particularly interesting from the experimental point of view, i.e. the wavenumbers of the stretching vibrational mode of Xe–H, $\nu_{\text{Xe-H}}$, and the stretching vibrational mode of H–X, $\nu_{\text{H-X}}$. The point of this discussion is to analyse the influence of the complexation on each property. The results of $\nu_{\text{Xe-H}}$ are collected in Tables II to VI and the wavenumbers for $\nu_{\text{H-X}}$ are collected in Tables VII to XI. We present experimental values of the complexation effect from the literature and the effect as accounted for by the MP2 and B3LYP methods.

1. Xe–H stretching mode

As seen in Tables II–VI, 32 of 41 structures studied exhibit a blue shift of the Xe–H stretching mode. In accordance with previous studies [14, 15, 31, 33, 35, 36], this shows that this behaviour is typical for the investigated compounds, even when the noble-gas molecule is not the proton donor. There are a couple of methodological points to make. First, the DFT/B3LYP/aug-cc-pVTZ(-PP) model seems not to perform well because it predicts red shifts for some of the structures, e.g. HXeCl$\cdots$HCl/1 while the blue shifts seem experimentally confirmed. Secondly, although our monomer wavenumber values are overestimated by about 200 cm^{-1} compared to the reported experimental results, the blue-shift values are under a minor influence of anharmonicity. For example, Lignell et al. [14] have studied the HXeY$\cdots$HX complexes for Y, X = Cl and Br. This study reported the experimental range observed for the blue-shifted $\nu_{\text{Xe-H}}$ for HXeCl$\cdots$HCl from 30.1–115.5 cm^{-1}. Their harmonic computational results for the same range are 10–117 cm^{-1} which is in excellent agreement with our MP2 anharmonic results: 8–109 cm^{-1} (see Tab.III). The results for HXeCl$\cdots$HBr and HXeBr$\cdots$HBr and HXeBr$\cdots$HCl compare equally well (see Tab.IV).

The blue-shifts are the largest for the structures of type 3 which corresponds to their largest interaction energy discussed above. Their values range from 106 to 154 cm^{-1}. The largest blue-shifts are observed for complexes containing HF. The shifts for geometries of type 1 and 2 of all compositions are positive and range from a couple of units to 59 cm^{-1}. The

only exception to this blue-shifting tendency are the complexes with HI which, according to our anharmonic results, mostly exhibit a red shift.

The curious exception of complexes with HI is puzzling. We do not observe any drastic differences between this complex and the others in terms of interaction energy components. However, the HXeCl$\cdots$HI/3 complex is the least stable in the HXeCl$\cdots$HX/3 group. HI also has the smallest dipole moment. From the HXeCl$\cdots$HI complexes, the HXeCl$\cdots$HI/2 structure has the lowest interaction energy and the largest red-shift of -365 cm^{-1}. Zhu et al. [36] mention that no evidence of HXeCl$\cdots$HI complex was noticed but their calculations predicted a blue shift. Our results suggest that the peaks corresponding to complexes with HI should be sought for wavenubers lower than the noble-gas-molecule. Tsuge et al. [35] did indeed find computationally a red-shifting H–Xe stretching mode but only for the structure of type 2 of HXeI$\cdots$HI and dihydrogen-bonded structure non studied here. Perhaps in the case of HI and lower interaction energies, the same effect that causes the blue shift of ν_{XeH} for other complexes does not occur. On the other hand, some part of the interaction mechanism could have not been accounted for in our calculations (e.g. a better description of relativistic effects), in which case the red-shift should be attributed to a defect in our computational model.

The results for complexes with HXeF provide two more red-shifting cases, namely the HXeF$\cdots$HBr/2 and HXeF$\cdots$HCl/3 structures, the first one, however, has a red shift of -3 cm^{-1} which may be a computational artifact. The latter complex red-shifts substantially, but there are no experimental data to refer to. In general, we were not successful in finding all the structures for HXeF complexes, but for those reported in Tab.II the observed trends are similar to the other noble-gas molecules.

2. Hydrogen halide HY stretching mode

The other interesting vibrational mode is that of the HX molecule. From Tables VII to XI one can see that all the $\nu_{\mathrm{H\text{-}X}}$ modes red-shift and the magnitude of the complexation effect corresponds to the intermolecular interaction energy. Consequently, the HXeCl/Br/I structures of type 3, in which HX is the proton donor, show the highest red shifts, approximately -300 to -500 cm^{-1}, while the structures of type 1 and 2 range from a few to approximately -40 cm^{-1}. In HXeF complexes, which were not synthesised, the computational red shift of

HF reaches -1000 cm^{-1}.

This trend can be seen in each subset of the structures of type 1, except for the HXeF molecule. For example, in the complexes HXeCl$\cdots$HCl/HBr/HI, the red shift increases as the interaction energy increases. This trend is reversed for the structures of type 2.

The obtained red-shift values for HXeI complex are in agreement with previous experimental studies. For instance, the change registered by Zhu et al. for HXeI$\cdots$HCl/3 (see Ref. [36], Tab.V) is -337 cm^{-1} and our anharmonic value is equal to -357 $^{-1}$. The experimental shift for the complex of type 3 with HBr is -378 cm^{-1} [35] and our calculations provide the value of -363 cm^{-1}. Our results could be used as a corroboration of the experimental assignments from the literature. For example, Tsuge et al. suggest another ν_{HBr} band which is blue-shifted by -266 cm^{-1} but this value is quite far from the anharmonic results. Similarly, the same authors observe the blue shift of -167 cm^{-1} for HI in complex with HXeI/3 but we predict a number twice as large, -347 cm^{-1}.

The red shifts of $\nu_{\mathrm{H\text{-}F}}$ for complexes with the HXeF molecule, as predicted by our calculations, are very large: -863 cm^{-1} for HXeF$\cdots$HF/3 and even -1001 cm^{-1} in the case of HXeF$\cdots$HCl/3. The former value compares quite well with a previous study by Yen et al. [60]. These authors obtained a red shift of -668 cm^{-1} for HXeF$\cdots$HF/3. Jankowska and Sadlej [38] report a value of -728 cm^{-1}.

IV. CONCLUSIONS

A structural search, an analysis of the intermolecular interaction energy, and an anharmonic Xe-H and H-X stretching vibrational mode analysis for the total of 41 different complexes of the formula HXeY$\cdots$HX was performed. We reported new structures of the complexes and found that different structures exhibit characteristic patterns in terms of electrostatic/induction/dispersion contributions to the total intermolecular interaction energy:

1. The structures of type 1 are mostly stabilized by dispersion interaction.

2. The structures of type 2 have large contributions from all three types of interaction, but since the first-order energy is repulsive, the second-order terms are the most important in stabilization.

3. The structures of type 3 are induction-dispersion stabilized and induction plays a

major role.

4. The structures of types 2a and 3a are outliers to these patterns: the electrostatic energy has the largest values of all. From the 2nd-order terms, induction is more important for structures 3a, while dispersion is slightly more important in the case of structures 2a.

Almost all of the studied structures exhibit a blue shift of the Xe–H stretching vibrational mode except for most of the complexes of HI and the complexes of HXeF. The magnitude of the complexation effect roughly correlates with the magnitude of the interaction, induction-stabilized complexes showing the largest shift. The stretching vibrational mode of H–X is found to red-shift and this effect is the largest for the type 3 structures.

ACKNOWLEDGMENTS

Computational resources at CSC - IT Center for Science Ltd. (Espoo, Finland) are acknowledged under project JY2535. This work was also supported by The National Science Centre (Poland, grant no. 2011/03/D/ST4/01341); and the Interdisciplinary Centre for Mathematical and Computational Modeling of the University of Warsaw (grant no. G56-12). Calculations have been carried out using resources provided by Wroclaw Centre for Networking and Supercomputing (https://wcss.pl), grant No. 321.

---

[1] N. Bartlett, Xenon Hexafluoroplatinate(v) $Xe^{+}[PtF_6]^{-}$, Proceedings of the Chemical Society **197–236**, 218 (1962).

[2] L. Graham, O. Graudejus, N. K. Jha, and N. Bartlett, Concerning the nature of $XePtF_6$, Coordination Chemistry Reviews **197**, 321 (2000).

[3] F. Grandinetti, 60 years of chemistry of the noble gases, Nature **606**, 659 (2022).

[4] R. Gerber, Formation of novel rare-gas molecules in low-temperature matrices, Annual Review of Physical Chemistry **55**, 55 (2004).

[5] L. Khriachtchev, M. Räsänen, and R. B. Gerber, Noble-Gas Hydrides: New Chemistry at Low Temperatures, Accounts of Chemical Research **42**, 183 (2009).

[6] W. Grochala, Atypical compounds of gases, which have been called 'noble', Chemical Society Reviews **36**, 1632 (2007).

[7] M. Pettersson, J. Lundell, and M. Räsänen, Neutral rare-gas containing charge-transfer molecules in solid matrices. I. HXeCl, HXeBr, HXeI, and HKrCl in Kr and Xe, The Journal of Chemical Physics **102**, 6423 (1995).

[8] M. Pettersson, J. Lundell, L. Khriachtchev, E. Isoniemi, and M. Räsänen, HXeSH, the First Example of a Xenon-Sulfur Bond, Journal of the American Chemical Society **120**, 7979 (1998).

[9] M. Pettersson, J. Lundell, and M. Räsänen, New Rare-Gas-Containing Neutral Molecules, European Journal of Inorganic Chemistry **1999**, 729 (1999).

[10] M. Pettersson, L. Khriachtchev, J. Lundell, and M. Räsänen, A Chemical Compound Formed from Water and Xenon: HXeOH, Journal of the American Chemical Society **121**, 11904 (1999).

[11] L. Khriachtchev, M. Pettersson, N. Runeberg, J. Lundell, and M. Räsänen, A stable argon compound, Nature **406**, 874 (2000).

[12] N. Runeberg, M. Pettersson, L. Khriachtchev, J. Lundell, and M. Räsänen, A theoretical study of HArF, a newly observed neutral argon compound, The Journal of Chemical Physics **114**, 836 (2001).

[13] A. Mohajeri and N. Bitaab, Investigating the nature of intermolecular and intramolecular bonds in noble gas containing molecules, International Journal of Quantum Chemistry **115**, 165 (2015).

[14] A. Lignell, J. Lundell, L. Khriachtchev, and M. Räsänen, Experimental and Computational Study of HXeY$\cdots$HX Complexes (X, Y = Cl and Br): An Example of Exceptionally Large Complexation Effect, The Journal of Physical Chemistry A **112**, 5486 (2008).

[15] G. Zhang, Y. Su, X. Zou, L. Fu, J. Song, D. Chen, and C. Sun, Charge-Shift Bonding in Xenon Hydrides: An NBO/NRT Investigation on HXeY$\cdots$HX (Y = Cl, Br, I; X = OH, Cl, Br, I, CCH, CN) via H-Xe Blue-Shift Phenomena, Frontiers in Chemistry **8**, 277 (2020).

[16] J. Lundell, M. Pettersson, and M. Räsänen, Computer experiments on xenon-containing molecules, Computers & Chemistry **24**, 325 (2000).

[17] A. V. Nemukhin, B. L. Grigorenko, L. Khriachtchev, H. Tanskanen, M. Pettersson, and M. Räsänen, Intermolecular Complexes of HXeOH with Water: Stabilization and Destabilization Effects, Journal of the American Chemical Society **124**, 10706 (2002).

[18] R. B. Gerber, E. Tsivion, L. Khriachtchev, and M. Räsänen, Intrinsic lifetimes and kinetic

stability in media of noble-gas hydrides, Chemical Physics Letters **545**, 1 (2012).

[19] E. Tsivion and R. B. Gerber, Lifetimes of compounds made of noble-gas atoms with water, Chemical Physics Letters **482**, 30 (2009).

[20] A. Lignell and L. Khriachtchev, Intermolecular interactions involving noble-gas hydrides: Where the blue shift of vibrational frequency is a normal effect, Journal of Molecular Structure **889**, 1 (2008).

[21] C. Sanloup, B. C. Schmidt, E. M. C. Perez, A. Jambon, E. Gregoryanz, and M. Mezouar, Retention of Xenon in Quartz and Earth's Missing Xenon, Science **310**, 1174 (2005).

[22] C. Leroy, C. Sanloup, H. Bureau, B. C. Schmidt, Z. Konôpková, and C. Raepsaet, Bonding of xenon to oxygen in magmas at depth, Earth and Planetary Science Letters **484**, 103 (2018).

[23] F. Peng, X. Song, C. Liu, Q. Li, M. Miao, C. Chen, and Y. Ma, Xenon iron oxides predicted as potential Xe hosts in Earth's lower mantle, Nature Communications **11**, 5227 (2020).

[24] M. J. Barlow, B. M. Swinyard, P. J. Owen, J. Cernicharo, H. L. Gomez, R. J. Ivison, O. Krause, T. L. Lim, M. Matsuura, S. Miller, G. Olofsson, and E. T. Polehampton, Detection of a Noble Gas Molecular Ion, $^{36}ArH^{+}$, in the Crab Nebula, Science **342**, 1343 (2013).

[25] R. A. Loomis, B. A. McGuire, C. Shingledecker, C. H. Johnson, S. Blair, A. Robertson, and A. J. Remijan, INVESTIGATING THE MINIMUM ENERGY PRINCIPLE IN SEARCHES FOR NEW MOLECULAR SPECIESTHE CASE OF H2C3O ISOMERS, The Astrophysical Journal **799**, 34 (2015).

[26] R. D. Sanders, N. P. Franks, and M. Maze, Xenon: No stranger to anaesthesia, British Journal of Anaesthesia **91**, 709 (2003).

[27] R. D. Sanders, D. Ma, and M. Maze, Xenon: Elemental anaesthesia in clinical practice, British Medical Bulletin **71**, 115 (2005).

[28] N. N. Andrijchenko, A. Y. Ermilov, L. Khriachtchev, M. Räsänen, and A. V. Nemukhin, Toward Molecular Mechanism of Xenon Anesthesia: A Link to Studies of Xenon Complexes with Small Aromatic Molecules, The Journal of Physical Chemistry A **119**, 2517 (2015).

[29] J. Cukras and J. Sadlej, Towards Quantum-Chemical Modeling of the Activity of Anesthetic Compounds, International Journal of Molecular Sciences **22**, 9272 (2021).

[30] W. Kossel, Über Molekülbildung als Frage des Atombaus, Annalen der Physik **354**, 229 (1916).

[31] J. Cukras and J. Sadlej, Theoretical predictions of the spectroscopic parameters in noble-gas molecules: HXeOH and its complex with water, Physical Chemistry Chemical Physics **13**,

15455 (2011).

[32] M. Tsuge, S. Berski, M. Räsänen, Z. Latajka, and L. Khriachtchev, Matrix-isolation and computational study of the HXeY$\cdots$H$_2$O complexes (Y = Cl, Br, and I), The Journal of Chemical Physics **140**, 044323 (2014).

[33] M. Tsuge, M. Räsänen, and L. Khriachtchev, Thermal decomposition of the HXeCl$\cdots$H$_2$O complex in solid xenon: Experimental characterization of the two-body decomposition channel, Chemical Physics Letters **739**, 136987 (2020).

[34] J. Cukras and J. Sadlej, The influence of the dispersion corrections on the performance of DFT method in modeling HNgY noble gas molecules and their complexes, Chemical Physics Letters **691**, 319 (2018).

[35] M. Tsuge, S. Berski, M. Räsänen, Z. Latajka, and L. Khriachtchev, Experimental and computational study of the HXeI$\cdots$HY complexes (Y = Br and I), The Journal of Chemical Physics **138**, 104314 (2013).

[36] C. Zhu, M. Tsuge, M. Räsänen, and L. Khriachtchev, Experimental and theoretical study of the HXeI$\cdots$HCl and HXeI$\cdots$HCCH complexes, The Journal of Chemical Physics **142**, 144306 (2015).

[37] C. Cheng and L. Sheng, Ab initio study of HXeF dimer and trimer, Computational and Theoretical Chemistry **989**, 39 (2012).

[38] J. Jankowska and J. Sadlej, Spectroscopic parameters in noble gas molecule: HXeF and its complex with HF, Chemical Physics Letters **517**, 155 (2011).

[39] E. Makarewicz, A. J. Gordon, K. Mierzwicki, Z. Latajka, and S. Berski, Effects of Xenon Insertion into Hydrogen Bromide. Comparison of the Electronic Structure of the HBr$\cdots$CO$_2$ and HXeBr$\cdots$CO$_2$ Complexes Using Quantum Chemical Topology Methods: Electron Localization Function, Atoms in Molecules and Symmetry Adapted Perturbation Theory, The Journal of Physical Chemistry A **118**, 3980 (2014).

[40] J. Cukras, G. Skóra, J. Jankowska, and J. Lundell, Computational Structures and SAPT Interaction Energies of HXeSH$\cdots$H$_2$Y (Y=O or S) Complexes, Inorganics **6**, 100 (2018).

[41] B. Jeziorski, R. Moszynski, and K. Szalewicz, Perturbation Theory Approach to Intermolecular Potential Energy Surfaces of van der Waals Complexes, Chemical Reviews **94**, 1887 (1994).

[42] A. J. Barnes and Z. Mielke, Matrix effects on hydrogen-bonded complexes trapped in low-temperature matrices, Journal of Molecular Structure **1023**, 216 (2012).

[43] M. J. Frisch, G. W. Trucks, H. B. Schlegel, G. E. Scuseria, M. A. Robb, J. R. Cheeseman, G. Scalmani, V. Barone, B. Mennucci, G. A. Petersson, H. Nakatsuji, M. Caricato, X. Li, H. P. Hratchian, A. F. Izmaylov, J. Bloino, G. Zheng, J. L. Sonnenberg, M. Hada, M. Ehara, K. Toyota, R. Fukuda, J. Hasegawa, M. Ishida, T. Nakajima, Y. Honda, O. Kitao, H. Nakai, T. Vreven, J. A. Montgomery, Jr., J. E. Peralta, F. Ogliaro, M. Bearpark, J. J. Heyd, E. Brothers, K. N. Kudin, V. N. Staroverov, R. Kobayashi, J. Normand, K. Raghavachari, A. Rendell, J. C. Burant, S. S. Iyengar, J. Tomasi, M. Cossi, N. Rega, J. M. Millam, M. Klene, J. E. Knox, J. B. Cross, V. Bakken, C. Adamo, J. Jaramillo, R. Gomperts, R. E. Stratmann, O. Yazyev, A. J. Austin, R. Cammi, C. Pomelli, J. W. Ochterski, R. L. Martin, K. Morokuma, V. G. Zakrzewski, G. A. Voth, P. Salvador, J. J. Dannenberg, S. Dapprich, A. D. Daniels, Ö. Farkas, J. B. Foresman, J. V. Ortiz, J. Cioslowski, and D. J. Fox, Gaussian∼09 Revision E.01.

[44] H.-J. Werner, P. J. Knowles, F. R. Manby, J. A. Black, K. Doll, A. Heßelmann, D. Kats, A. Köhn, T. Korona, D. A. Kreplin, Q. Ma, T. F. Miller, A. Mitrushchenkov, K. A. Peterson, I. Polyak, G. Rauhut, and M. Sibaev, The Molpro quantum chemistry package, The Journal of Chemical Physics **152**, 144107 (2020).

[45] R. A. Kendall, T. H. Dunning, and R. J. Harrison, Electron affinities of the first-row atoms revisited. Systematic basis sets and wave functions, Journal of Chemical Physics **96**, 6796 (1992).

[46] T. H. Dunning, Gaussian basis sets for use in correlated molecular calculations. I. The atoms boron through neon and hydrogen, Journal of Chemical Physics **90**, 1007 (1989).

[47] D. E. Woon and T. H. Dunning, Gaussian basis sets for use in correlated molecular calculations. III. The atoms aluminum through argon, Journal of Chemical Physics **98**, 1358 (1993).

[48] A. K. Wilson, D. E. Woon, K. A. Peterson, and T. H. Dunning, Gaussian basis sets for use in correlated molecular calculations. IX. The atoms gallium through krypton, Journal of Chemical Physics **110**, 7667 (1999).

[49] K. A. Peterson, D. Figgen, E. Goll, H. Stoll, and M. Dolg, Systematically convergent basis sets with relativistic pseudopotentials. II. Small-core pseudopotentials and correlation consistent basis sets for the post-d group 16-18 elements, Journal of Chemical Physics **119**, 11113 (2003).

[50] K. A. Peterson, B. C. Shepler, D. Figgen, and H. Stoll, On the spectroscopic and thermochemical properties of ClO, BrO, IO, and their anions, Journal of Physical Chemistry A **110**, 13877 (2006).

[51] B. P. Pritchard, D. Altarawy, B. Didier, T. D. Gibson, and T. L. Windus, New Basis Set Exchange: An Open, Up-to-Date Resource for the Molecular Sciences Community, Journal of Chemical Information and Modeling **59**, 4814 (2019).

[52] S. F. Boys and F. Bernardi, The calculation of small molecular interactions by the differences of separate total energies. Some procedures with reduced errors, Molecular Physics 10.1080/00268977000101561 (2006).

[53] F. Pérez and B. E. Granger, IPython: A system for interactive scientific computing, Computing in Science and Engineering **9**, 21 (2007).

[54] T. Kluyver, B. Ragan-Kelley, F. Pérez, B. Granger, M. Bussonnier, J. Frederic, K. Kelley, J. Hamrick, J. Grout, S. Corlay, P. Ivanov, D. Avila, n, S. Abdalla, C. Willing, and J. D. Team, Jupyter Notebooks – a publishing format for reproducible computational workflows, Positioning and Power in Academic Publishing: Players, Agents and Agendas , 87 (2016).

[55] J. D. Hunter, Matplotlib: A 2D Graphics Environment, Computing in Science Engineering **9**, 90 (2007).

[56] J. Reback, jbrockmendel, W. McKinney, J. V. den Bossche, T. Augspurger, P. Cloud, S. Hawkins, gfyoung, Sinhrks, M. Roeschke, A. Klein, T. Petersen, J. Tratner, C. She, W. Ayd, P. Hoefler, S. Naveh, M. Garcia, J. Schendel, A. Hayden, D. Saxton, R. Shadrach, M. E. Gorelli, V. Jancauskas, F. Li, attack68, A. McMaster, P. Battiston, S. Seabold, and K. Dong, Pandas-dev/pandas: Pandas 1.3.1, Zenodo (2021).

[57] W. McKinney, Data Structures for Statistical Computing in Python, Proceedings of the 9th Python in Science Conference , 56 (2010).

[58] A. Mukhopadhyay, S. S. Xantheas, and R. J. Saykally, The water dimer II: Theoretical investigations, Chemical Physics Letters **700**, 163 (2018).

[59] J. R. Lane, CCSDTQ Optimized Geometry of Water Dimer, Journal of Chemical Theory and Computation **9**, 316 (2013).

[60] S.-Y. Yen, C.-H. Mou, and W.-P. Hu, Strong hydrogen bonding between neutral noble-gas molecules (HNgF, Ng=Ar, Kr, and Xe) and hydrogen fluoride: A theoretical study, Chemical Physics Letters **383**, 606 (2004).

TABLE I: The supermolecular interaction energy values obtained with HF, MP2, MP4, CCSD and CCSD(T) methods and the total SAPT interaction energy of all examined structures, given in kJ·mol^{-1}

Complex/structure type	SAPT	HF	MP2	MP4	CCSD	CCSD(T)
HXeF··· HF/1	-11.04	-7.48	-7.57	-6.97	-7.54	-7.39
HXeF··· HCl/1	-8.03	1.19	-3.69	-2.99	-2.41	-2.92
HXeF··· HBr/1	-17.63	-3.29	-9.37	-8.45	-7.73	-8.32
HXeCl··· HCl/1	-7.54	2.95	-4.61	-3.14	-2.07	-2.80
HXeCl··· HBr/1	-18.00	1.45	-9.07	-6.97	-5.45	-6.41
HXeCl··· HI/1	-32.62	-1.63	-14.18	-11.36	-9.42	-10.58
HXeBr··· HCl/1	-7.59	3.33	-4.75	-3.16	-2.00	-2.76
HXeBr··· HBr/1	-19.03	2.37	-8.93	-6.65	-4.99	-6.01
HXeBr··· HI/1	-36.00	-0.04	-13.72	-10.67	-8.53	-9.77
HXeI··· HCl/1	-7.37	3.52	-4.74	-3.05	-1.83	-2.61
HXeI··· HBr/1	-19.28	3.21	-8.41	-6.00	-4.23	-5.28
HXeI··· HI/1	-37.75	1.63	-12.65	-9.41	-7.11	-8.40
HXeF··· HCl/2	-5.48	-0.53	-3.79	-2.58	-2.40	-2.66
HXeF··· HBr/2	-6.32	0.58	-3.88	-2.57	-2.15	-2.54
HXeCl··· HCl/2	-6.25	-1.13	-5.30	-3.81	-3.17	-3.47
HXeCl··· HBr/2	-6.09	0.19	-5.69	-3.93	-2.96	-3.44
HXeCl··· HI/2	-9.25	1.57	-6.28	-4.13	-2.71	-3.43
HXeBr··· HCl/2	-6.08	-1.05	-4.97	-3.42	-2.76	-3.02
HXeBr··· HBr/2	-8.22	0.33	-5.43	-3.55	-2.52	-2.97
HXeBr··· HI/2	-10.16	1.85	-6.17	-3.78	-2.23	-2.93
HXeI··· HCl/2	-5.82	-1.00	-4.39	-2.75	-2.12	-2.30
HXeI··· HBr/2	-8.54	0.45	-4.93	-2.87	-1.80	-2.16
HXeI··· HI/2	-11.65	2.17	-5.89	-3.10	-1.38	-2.00
HXeF··· HF/3	-67.09	-65.91	-62.99	-59.53	-63.05	-61.96
HXeF··· HCl/3	-38.80	-41.08	-51.87	-46.10	-45.48	-46.36
HXeCl··· HF/3	-43.05	-35.43	-41.10	-39.13	-38.59	-38.83
HXeCl··· HCl/3	-26.02	-16.49	-32.85	-28.22	-25.54	-27.18
HXeCl··· HBr/3	-24.93	-10.66	-29.73	-24.64	-21.26	-23.33
HXeCl··· HI/3	-20.15	-2.81	-24.24	-18.71	-14.53	-17.10
HXeBr··· HF/3	-39.21	-29.81	-35.43	-33.54	-32.92	-33.17
HXeBr··· HCl/3	-26.28	-12.97	-28.92	-24.53	-21.89	-23.43
HXeBr··· HBr/3	-27.66	-7.84	-26.57	-21.70	-18.40	-20.35
HXeBr··· HI/3	-25.67	-0.95	-22.23	-16.88	-12.78	-15.22
HXeI··· HF/3	-33.30	-23.92	-28.90	-27.12	-26.46	-26.66
HXeI··· HCl/3	-22.91	-9.18	-24.01	-19.95	-17.42	-18.82
HXeI··· HBr/3	-25.56	-4.72	-22.48	-17.92	-14.71	-16.52
HXeI··· HI/3	-25.36	1.23	-19.30	-14.23	-10.23	-12.51
HXeF··· HF/2a	-10.31	-7.31	-6.91	-5.90	-6.72	-6.45
HXeCl··· HF/2a	-12.23	-9.64	-9.22	-8.21	-8.60	-8.23
HXeF··· HF/3a	-63.67	-63.86	-58.51	-55.56	-59.25	-57.86
HXeCl··· HF/3a	-31.87	-27.68	-29.32	-27.98	-28.04	-27.83

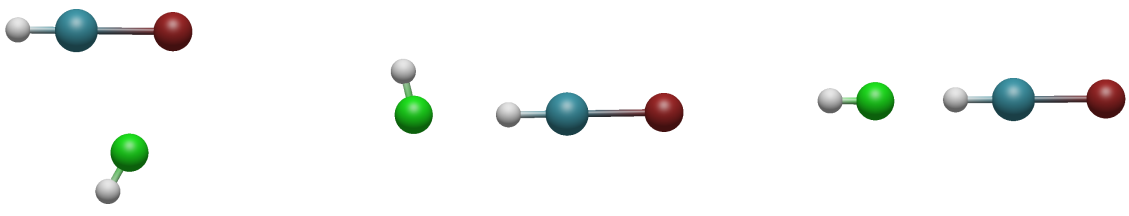

(a) Structure of type 1 (b) Structure of type 2 (c) Structure of type 2a

(d) Structure of type 3 (e) Structure of type 3a

FIG. 1: The obtained structure types of the HXeY···HX complexes. The elements are color-coded (H: white, Xe: teal, halogen in HX: green, halogen in HXeY: red)

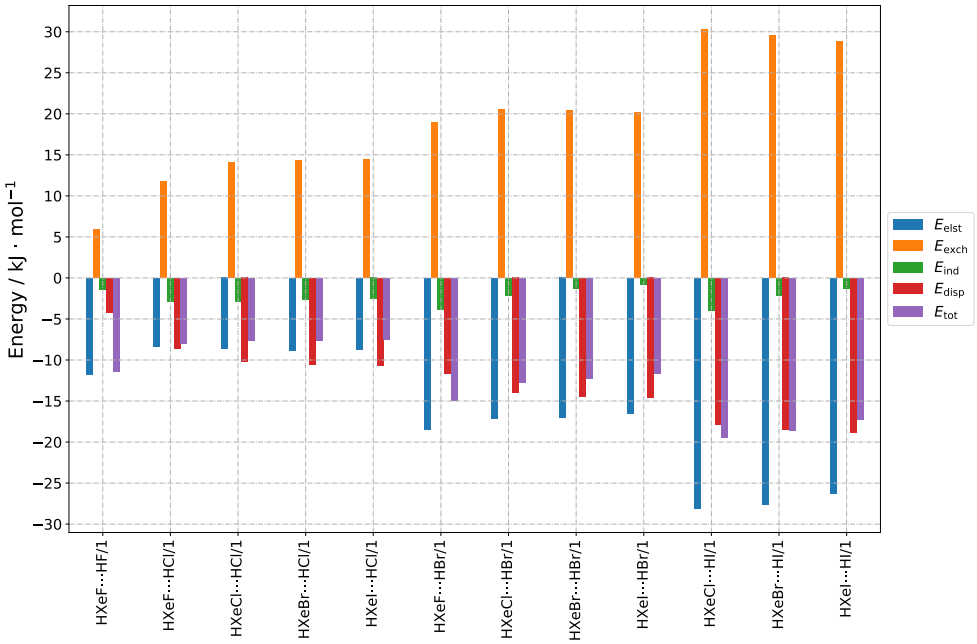

FIG. 2: Bar graphs depicting the SAPT decomposition of the intermolecular interaction energy for HXeY···HX complexes assuming structure of type 1. The graphs are grouped by HX molecule

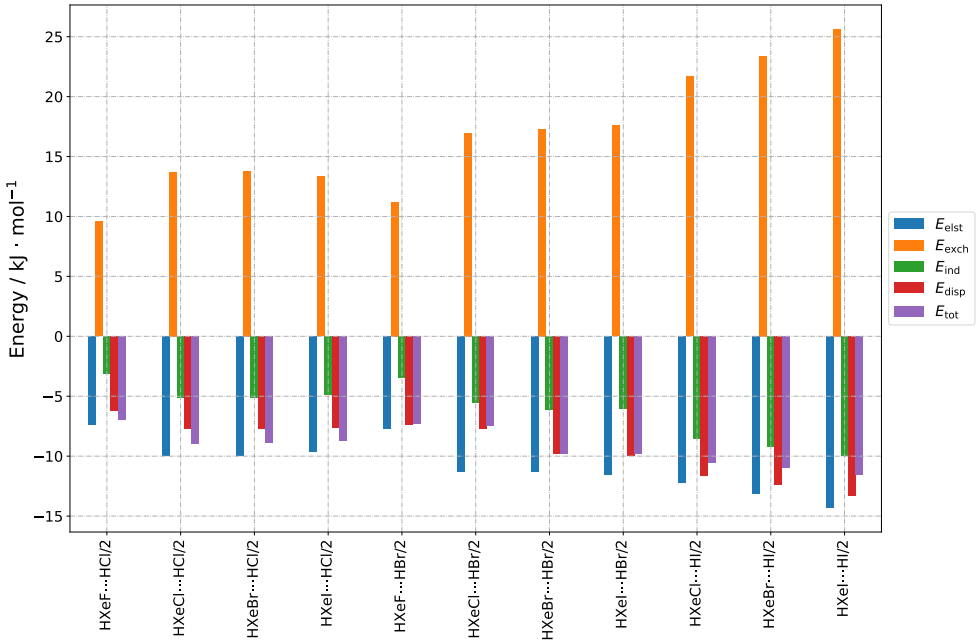

FIG. 3: Bar graphs depicting the SAPT decomposition of the intermolecular interaction energy for HXeY···HX complexes assuming structure of type 2. The graphs are grouped by HX molecule

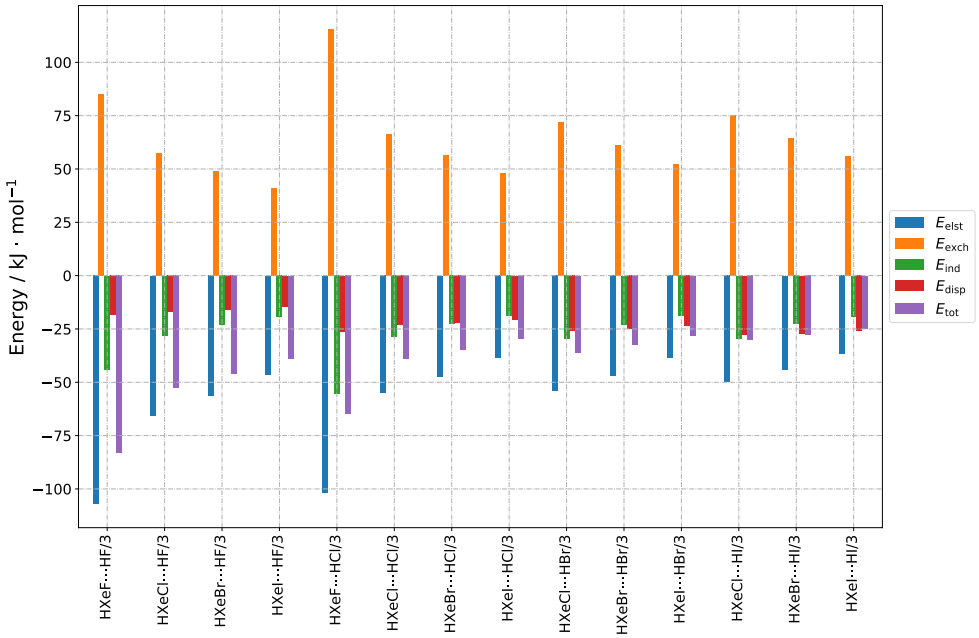

FIG. 4: Bar graphs depicting the SAPT decomposition of the intermolecular interaction energy for HXeY···HX complexes assuming structure of type 3. The graphs are grouped by HX molecule

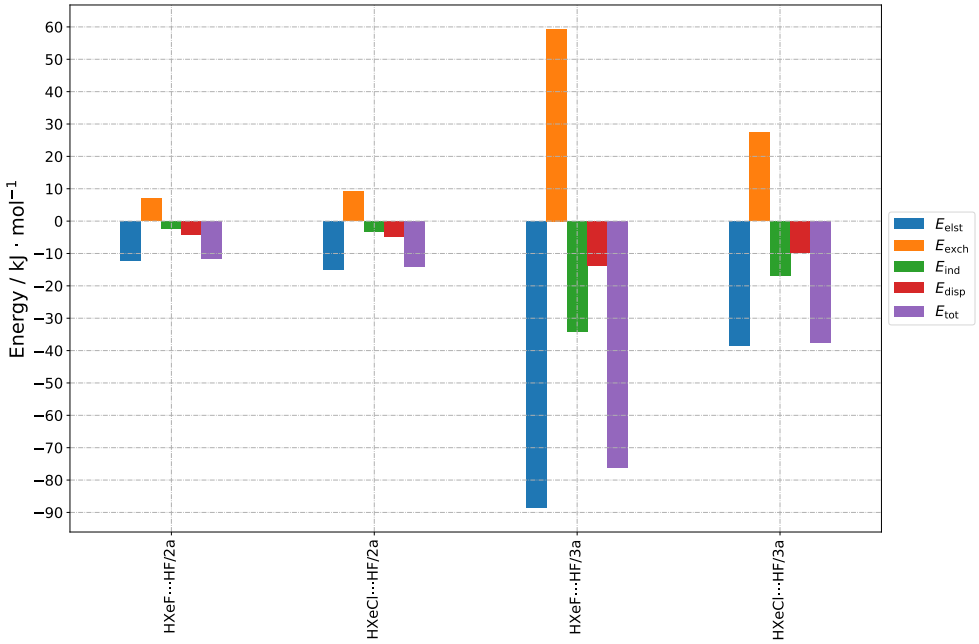

FIG. 5: Bar graphs depicting the SAPT decomposition of the intermolecular interaction energy for HXeY···HX complexes assuming structure of type 2a and 3a

TABLE II: The anharmonic $\nu_{\mathrm{Xe-H}}$ stretching vibration frequencies in the studied complexes in different structures of HXeF complexes. $\Delta\nu$ denotes the change in value compared to a non-interacting monomer. Values are given in cm^{-1}. There is no experimental value of $\nu_{\mathrm{Xe-H}}$ for the HXeF molecule

type	HX	ν(MP2)	$\Delta\nu$(MP2)	ν(B3LYP)	$\Delta\nu$(B3LYP)
1	HF	2037	29	#	#
	HCl	2010	2	1833	-81
	HBr	2022	14	1949	35
	HI	#	#	#	#
2	HF	#	#	#	#
	HCl	2020	12	1922	8
	HBr	2005	-3	1902	-12
	HI	#	#	#	#
3	HF	2127	119	1945	31
	HCl	1659	-349	1942	28
	HBr	#	#	#	#
	HI	#	#	#	#

TABLE III: The anharmonic $\nu_{\mathrm{Xe-H}}$ stretching vibration frequencies in the studied complexes in different structures of HXeCl complexes. $\Delta\nu$ denotes the change in value compared to a non-interacting monomer which equals 1648 cm^{-1} (experiment, see Refs. [7, 20]) and 1825 cm^{-1} (our anharmonic calculations). Values are given in cm^{-1}

type	HX	$\Delta\nu$(exp)[a]	ν(MP2)	$\Delta\nu$(MP2)	ν(B3LYP)	$\Delta\nu$(B3LYP)
1	HF	#	#	#	#	#
	HCl	30-50	1833	8	1730	-19
	HBr	#	1847	22	1759	10
	HI	#	1611	-214	1774	25
2	HF	#	#	#	#	#
	HCl	30-50	1857	32	1779	30
	HBr	#	1828	3	1720	-29
	HI	#	1460	-365	1603	-146
3	HF	#	1957	132	1831	82
	HCl	80-115	1934	109	1750	1
	HBr	#	1931	106	1858	109
	HI	#	1659	-166	1733	-16

TABLE IV: The anharmonic $\nu_{\mathrm{Xe-H}}$ stretching vibration frequencies in the studied complexes in different structures of HXeBr complexes. $\Delta\nu$ denotes the change in value compared to a non-interacting monomer which equals 1504 cm^{-1} (experiment, see Refs. [7, 20]) and 1710 cm^{-1} (our anharmonic calculations). Values are given in cm^{-1}

type	HX	$\Delta\nu$(exp)	ν(MP2)	$\Delta\nu$(MP2)	ν(B3LYP)	$\Delta\nu$(B3LYP)
1	HF	#	#	#	#	#
	HCl	#	1719	9	1668	101
	HBr	24-39	1734	24	1679	112
	HI	#	1755	45	1693	126
2	HF	#	#	#	#	#
	HCl	#	1755	45	#	#
	HBr	24-39	1729	19	1542	-25
	HI	#	1660	-50	1388	-179
3	HF	#	1852	142	1709	142
	HCl	80-120	1827	117	1668	101
	HBr	73-145	1826	116	1732	165
	HI	#	1774	64	1730	163

TABLE V: The anharmonic $\nu_{\mathrm{Xe-H}}$ stretching vibration frequencies in the studied complexes in different structures of HXeI complexes. $\Delta\nu$ denotes the change in value compared to a non-interacting monomer which equals 1193 cm^{-1} (experiment, see Refs. [7, 36]) and 1529 cm^{-1} (our anharmonic calculations). Values are given in cm^{-1}

type	HX	ν(exp)	ν(MP2)	$\Delta\nu$(MP2)	ν(B3LYP)	$\Delta\nu$(B3LYP)
1	HF		#	#	#	#
	HCl	94–155	1537	8	1361	-64
	HBr		1554	25	1383	-42
	HI		1279	-250	1391	-34
2	HF		#	#	#	#
	HCl	94–155	1588	59	#	#
	HBr		1571	42	1313	-112
	HI		1044	-485	1190	-235
3	HF		1683	154	1561	136
	HCl	94–155	1651	122	1533	108
	HBr		1650	121	1533	108
	HI		1330	-199	1506	81

TABLE VI: The anharmonic $\nu_{\mathrm{Xe-H}}$ stretching vibration frequencies in the studied complexes in different structures of type 2a and 3a. $\Delta\nu$ denotes the change in value compared to a non-interacting monomer. Values are given in cm^{-1}

type	structure	ν(MP2)	$\Delta\nu$(MP2)	ν(B3LYP)	$\Delta\nu$(B3LYP)
2a	HXeF$\cdots$FH	2024	16	#	#
	HXeCl$\cdots$FH	1881	56	#	#
3a	HXeF$\cdots$FH	2126	118	#	#
	HXeCl$\cdots$FH	1922	97	#	#

TABLE VII: The anharmonic $\nu_{\mathrm{X-H}}$ stretching vibration frequencies in the studied complexes in different structures of HXeF complexes. $\Delta\nu$ denotes the change in value compared to a non-interacting monomer. Values are given in cm^{-1}

type	HX	ν(MP2)	$\Delta\nu$(MP2)	ν(B3LYP)	$\Delta\nu$(B3LYP)
1	HF	3923	-29	#	#
	HCl	2932	-11	2808	-52
	HBr	2641	-23	2568	40
	HI	#	#	#	#
2	HF	#	#	#	#
	HCl	2931	-12	2855	-5
	HBr	2653	-11	2523	-5
	HI	#	#	#	#
3	HF	3089	-863	3019	-882
	HCl	1942	-1001	1862	-998
	HBr	#	#	#	#
	HI	#	#	#	#

TABLE VIII: The anharmonic $\nu_{\mathrm{X-H}}$ stretching vibration frequencies in the studied complexes in different structures of HXeCl complexes. $\Delta\nu$ denotes the change in value compared to a non-interacting monomer. Values are given in cm^{-1}

type	HX	ν(MP2)	$\Delta\nu$(MP2)	ν(B3LYP)	$\Delta\nu$(B3LYP)
1	HF	#	#	#	#
	HCl	2928	-15	2861	1
	HBr	2637	-27	2459	-69
	HI	2308	-38	2101	-105
2	HF	#	#	#	#
	HCl	#	#	2847	-13
	HBr	2651	-13	2524	-4
	HI	2337	-9	2209	3
3	HF	3370	-582	3302	-599
	HCl	#	#	2279	-581
	HBr	2174	-490	1942	-586
	HI	2024	-322	1776	-430

TABLE IX: The anharmonic $\nu_{\mathrm{X-H}}$ stretching vibration frequencies in the studied complexes in different structures of HXeBr complexes. $\Delta\nu$ denotes the change in value compared to a non-interacting monomer. Values are given in cm^{-1}

type	HX	ν(MP2)	$\Delta\nu$(MP2)	ν(B3LYP)	$\Delta\nu$(B3LYP)
1	HF	#	#	#	#
	HCl	2928	-15	2862	2
	HBr	2634	-30	2403	-125
	HI	2305	-41	2087	-119
2	HF	#	#	#	#
	HCl	2927	-16	#	#
	HBr	2651	-13	2524	-4
	HI	2336	-10	2205	-1
3	HF	3475	-477	3376	-525
	HCl	2522	-421	2363	-497
	HBr	2244	-420	1924	-604
	HI	1961	-385	1758	-448

TABLE X: The anharmonic $\nu_{\mathrm{X-H}}$ stretching vibration frequencies in the studied complexes in different structures of HXeI complexes. $\Delta\nu$ denotes the change in value compared to a non-interacting monomer. Values are given in cm^{-1}

type	HX	ν(MP2)	$\Delta\nu$(MP2)	ν(B3LYP)	$\Delta\nu$(B3LYP)
1	HF	#	#	#	#
	HCl	2926	-17	2868	8
	HBr	2633	-31	2367	-161
	HI	2303	-43	2204	-2
2	HF	#	#	#	#
	HCl	2928	-15	#	#
	HBr	2652	-12	2525	-3
	HI	2336	-10	2197	-9
3	HF	#	#	3443	-458
	HCl	2587	-356	2343	-517
	HBr	2301	-363	2073	-455
	HI	1999	-347	1749	-457

TABLE XI: The anharmonic $\nu_{\mathrm{X-H}}$ stretching vibration frequencies in the studied complexes in different structures of type 2a and 3a. $\Delta\nu$ denotes the change in value compared to a non-interacting monomer. Values are given in cm^{-1}

type	structure	ν(MP2)	$\Delta\nu$(MP2)	ν(B3LYP)	$\Delta\nu$(B3LYP)
2a	HXeFFH	3931	-21	#	#
	HXeClFH	3925	-27	#	#
3a	HXeFFH	3301	-651	#	#
	HXeClFH	3692	-260	#	#

TABLE XII: Dipole moment (in Debyes) of the HX and HXeY molecules

Dipole moments	HX	HXeY
H_2O	1.85	1.85
F	1.82	2.05
Cl	1.08	6.42
Br	0.82	6.45
I	0.44	6.1

V. APPENDIX: ADDITIONAL SAPT FIGURES

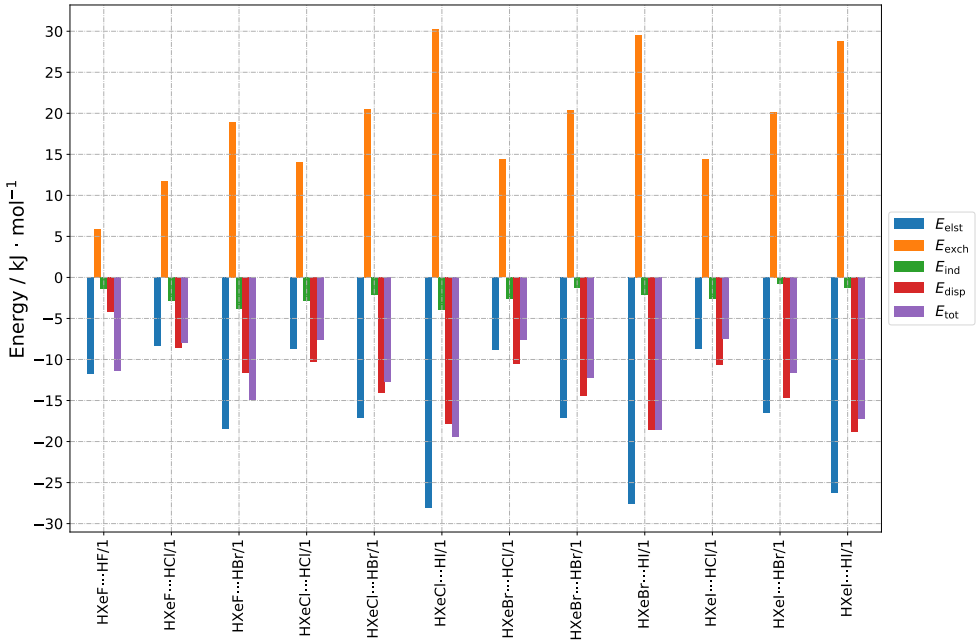

FIG. 6: Bar graphs depicting the SAPT decomposition of the intermolecular interaction energy for HXeY···HX complexes assuming structure of type 1. The graphs are grouped by HXeY molecule

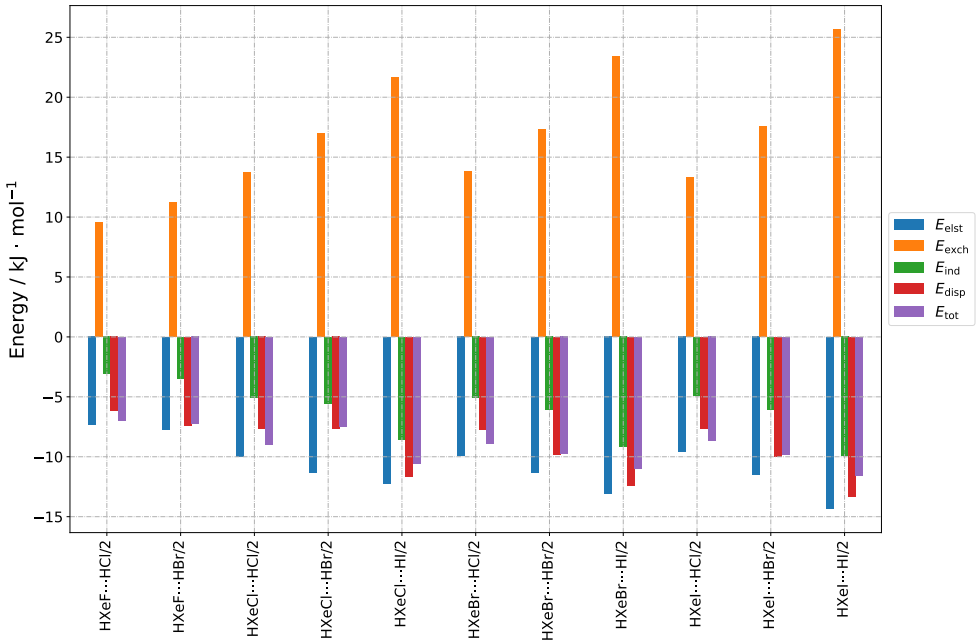

FIG. 7: Bar graphs depicting the SAPT decomposition of the intermolecular interaction energy for HXeY···HX complexes assuming structure of type 2. The graphs are grouped by HXeY molecule

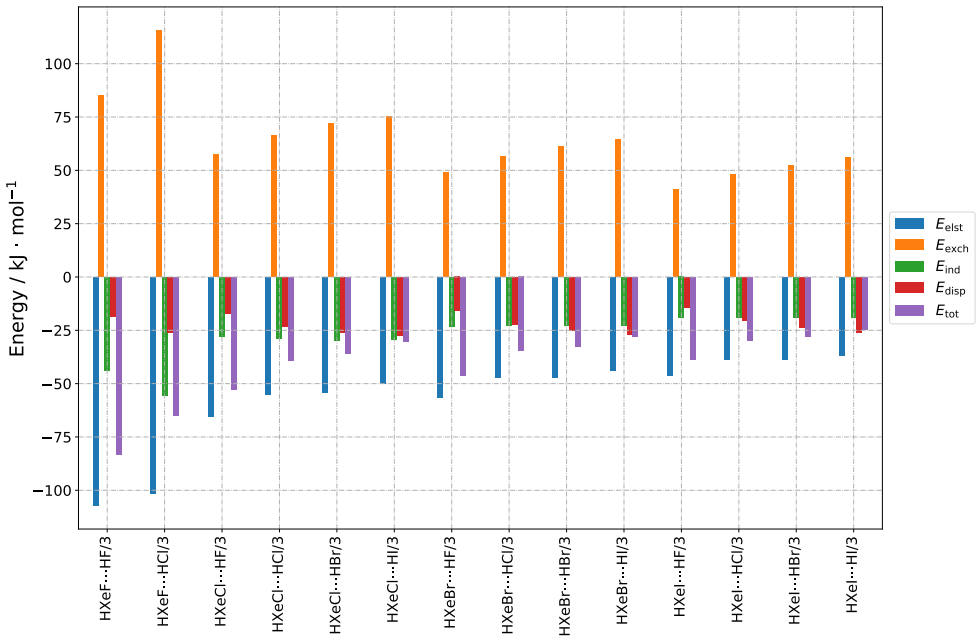

FIG. 8: Bar graphs depicting the SAPT decomposition of the intermolecular interaction energy for HXeY···HX complexes assuming structure of type 3. The graphs are grouped by HXeY molecule

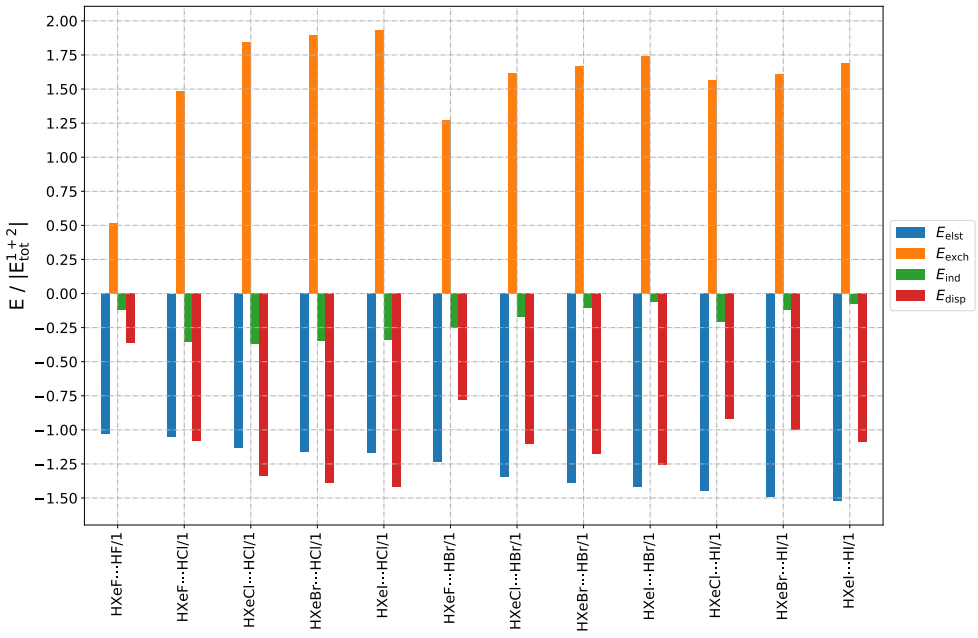

FIG. 9: Bar graphs depicting the SAPT decomposition of the intermolecular interaction energy using values relative to the total interaction energy for HXeY···HX complexes assuming structure of type 1. The graphs are grouped by HX molecule

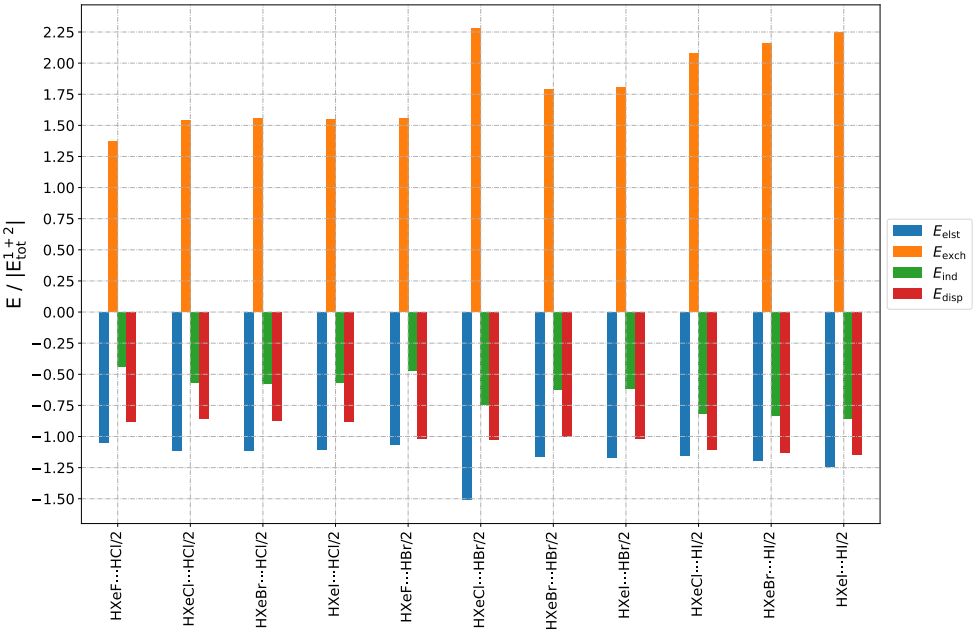

FIG. 10: Bar graphs depicting the SAPT decomposition of the intermolecular interaction energy using values relative to the total interaction energy for HXeY···HX complexes assuming structure of type 2. The graphs are grouped by HX molecule

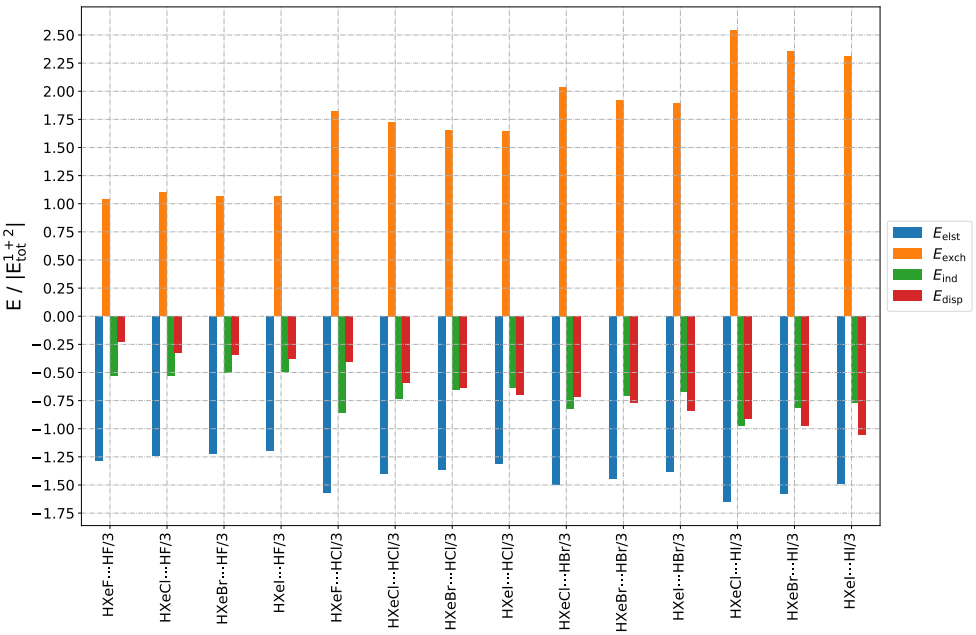

FIG. 11: Bar graphs depicting the SAPT decomposition of the intermolecular interaction energy using values relative to the total interaction energy for HXeY···HX complexes assuming structure of type 3. The graphs are grouped by HX molecule

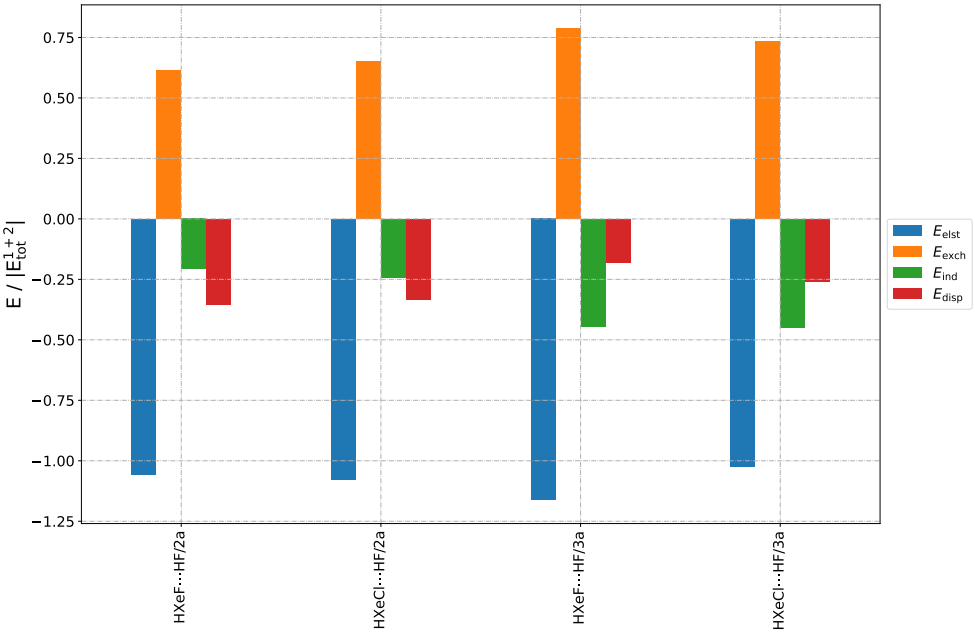

FIG. 12: Bar graphs depicting the SAPT decomposition of the intermolecular interaction energy using values relative to the total interaction energy for HXeY···HX complexes assuming structure of type 2a and 3a

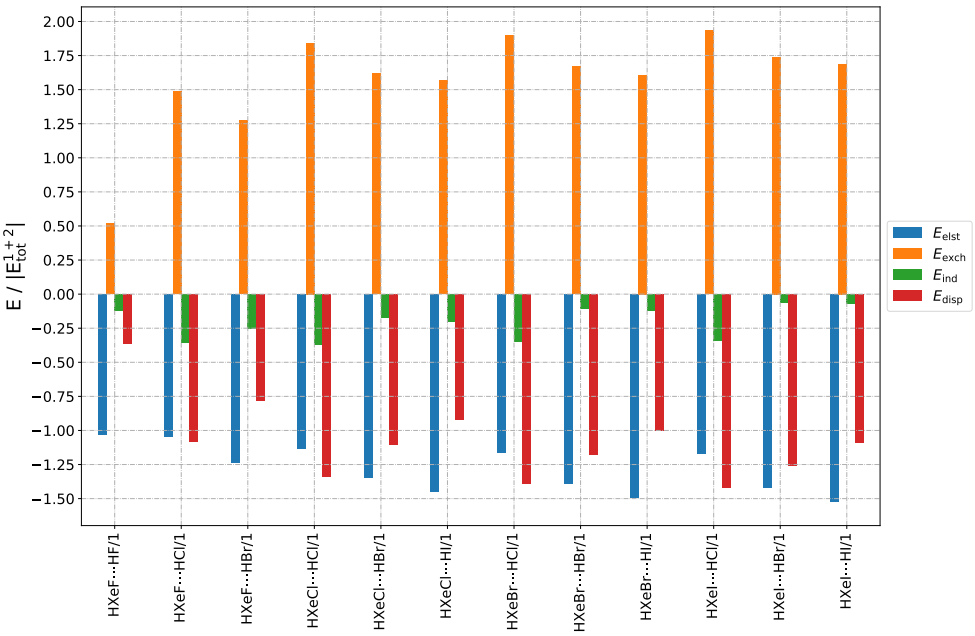

FIG. 13: Bar graphs depicting the SAPT decomposition of the intermolecular interaction energy using values relative to the total interaction energy for HXeY···HX complexes assuming structure of type 1. The graphs are grouped by HXeY molecule

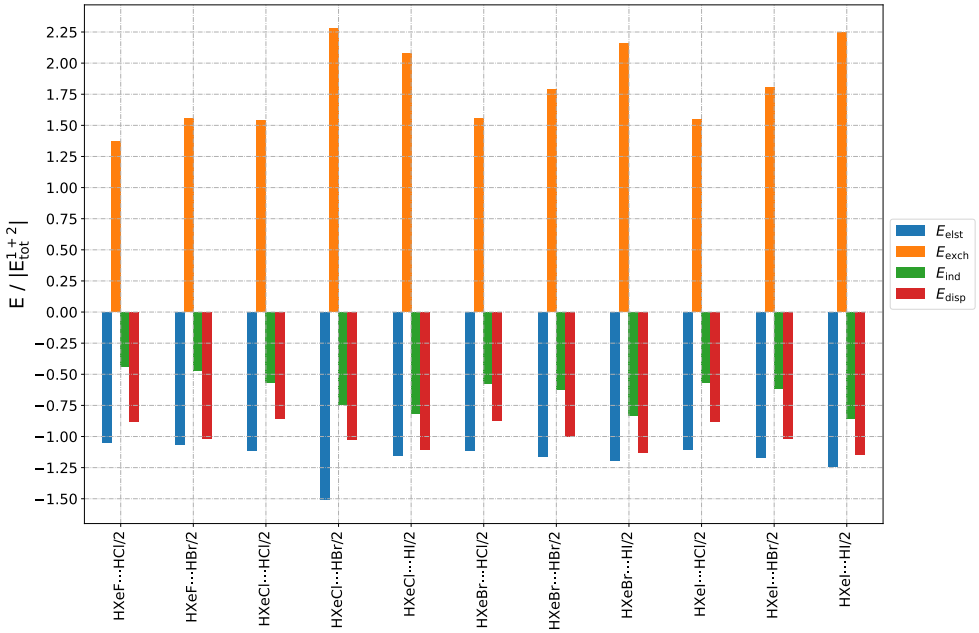

FIG. 14: Bar graphs depicting the SAPT decomposition of the intermolecular interaction energy using values relative to the total interaction energy for HXeY···HX complexes assuming structure of type 2. The graphs are grouped by HXeY molecule

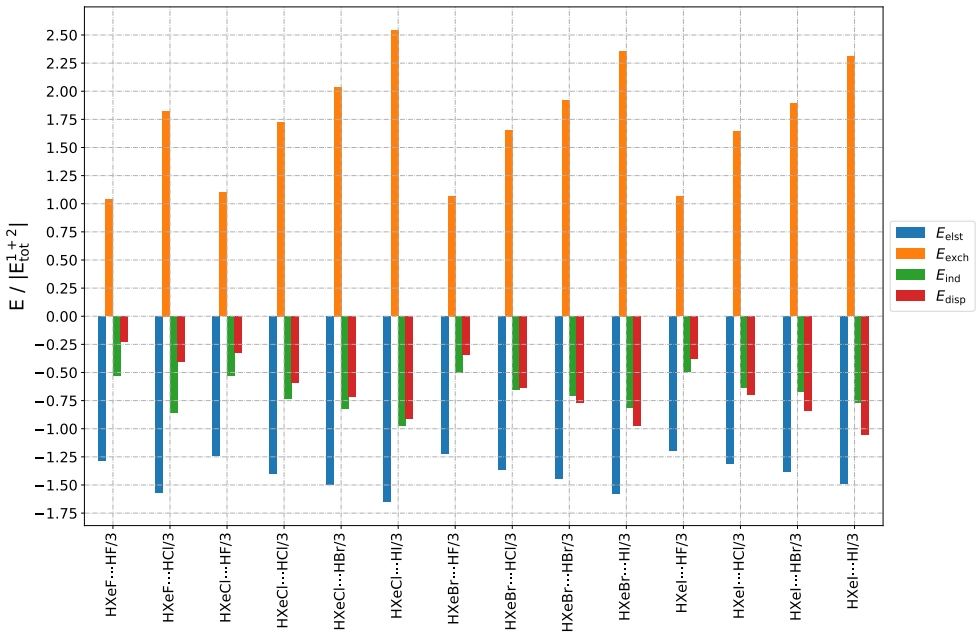

FIG. 15: Bar graphs depicting the SAPT decomposition of the intermolecular interaction energy using values relative to the total interaction energy for HXeY···HX complexes assuming structure of type 3. The graphs are grouped by HXeY molecule